Journal of the Korean Nuclear Society
Volume 32, Number 3, pp.227~234, June 2000

Development of a Mass Estimation Algorithm Using the Impact Test Data of Nuclear Power Plant

J. S. Kim, I .K. Hwang, D. Y. Lee, C. S. Ham, and T. H. Kim

Korea Atomic Energy Research Institute
150 Dukjin-dong, Yusong-gu, Taejon 305-353, Korea
kjs@kaeri.re.kr

(Received October 29, 1999)

Abstract

It is known that loose parts in the reactor coolant system (RCS) cause serious damage to the systems. This paper is concerned with estimating the mass of a loose part in the steam generator of a nuclear power plant. We developed the mass estimation algorithm based on the Hertz theory in order to estimate the mass of the loose parts and applied the algorithm to the impact test data of YGN3. The mass estimation values were compared with real values in order to verify the algorithm. The result showed that the average error of the mass estimation value is less than 27%.

Key Words : loose-part, mass, energy, diagnosis, impact test.

1. Introduction

LPMS is a diagnostic system that monitors the integrity of a Nuclear Steam Supply System (NSSS) and analyzes the impact of events caused by moving or loose parts. This system provides the necessary information for the operator' s proper decision to maintain a reliable and safe Nuclear Power Plant (NPP). The loose parts, metal pieces, are produced by being parted from the structure of the reactor coolant system (RCS) due to corrosion, fatigue, and friction between the components in the RCS and also by coming into the RCS from the outside during a period of reactor test operation, refueling, and overall maintenance. These loose parts are mixed with the reactor coolant fluid, move with high velocity along the RCS circuit, and generate collisions with RCS components. When a loose part strikes against the components within the pressure boundary, an acoustic impact wave is produced and propagates along the pressure boundary. For detecting the impact signal, a conventional LPMS uses the accelerometer sensors installed on the outer surface of the pressure boundary of the RCS components and announces an alarm when the detected impact signal exceeds a certain level which is pre-set by the operator. The sensors are

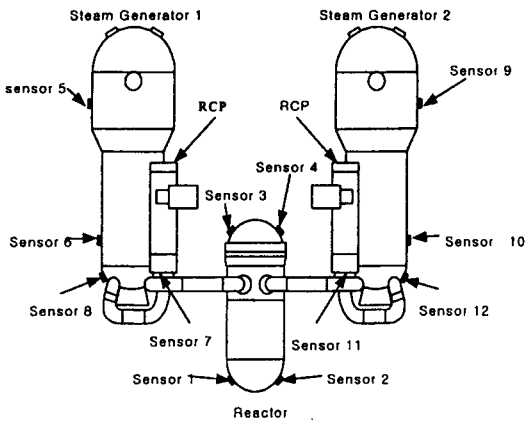

Fig. 1. Sensor Positions of NSSS at YGN 3&4

usually installed on the probable places where the loose parts may be collected such as the upper head of the reactor pressure vessel and the hot chamber of the Steam Generator [1]. Fig. 1 shows a typical arrangement of sensors at YGN 3&4 mounted on the outer surface of the major components of the NSSS, where the sensor locations are marked with a rectangular block. In the current LPMS, the alarm is triggered in the case where the signal threshold is exceeded by the measured signal and the detected signal is recorded on to magnetic tape. Later, the experienced operators analyze the recorded data and determine whether the detected signal is an impact signal by a loose part or a noise signal.

If they conclude that loose parts caused the signal, they evaluate the characteristic parameters such as the impact location, energy, and mass. After the diagnosis process is completed, the proper procedure required for maintaining safe and reliable operation is performed. In the conventional diagnostic method in LPMS, the operators should have expert knowledge for diagnosing the impact signal in order to execute the proper action. Moreover, it takes a long time to analyze the detected signal data and hence possibly fatal damage to components may occur during the analysis procedure. Therefore, it is very desirable that when the alarm is triggered by a loose part' s impact, the detected signal is stored in the computer memory, the automatic diagnosis procedure is activated immediately, and displays the diagnostic results such as location, mass and energy of a loose part on the operator' s monitors.

Generally, two methods for mass estimation have been known: one is a time series analysis and the other is a frequency analysis. In the time series analysis method, the Hertz theory is used to determine the loose parts impact signal model and the equation for plate wave propagation is derived [2-4]. But the theory is not directly applicable to real plants because of violations of the basic assumptions. For instance, the structure of a steam generator consists of two parts; the side is of a cylindrical shape and upper & lower parts of a hemisphere shape. The impact source is not the solid sphere. On the other hand, for the frequency analysis method [5-7], we should first change the impact (time) data to frequency data using Fast Fourier Transformations (FFT). From the frequency spectrum, we then find the characteristic frequency and estimate the mass referring to the look-up table. In this study, an automatic estimation algorithm of the mass of a loose part is developed using the time domain data and modifying the basic theory in a practical way. The present scheme is applied to the impact data of YGN 3. The experimental results show the good performance of the diagnosis algorithm. In this paper, Sec. 2 describes the flowchart of the developed algorithm based on the Hertz theory. Sec. 3 describes the experimental results applying to the YGN 3 impact test data. The last section is the conclusions.

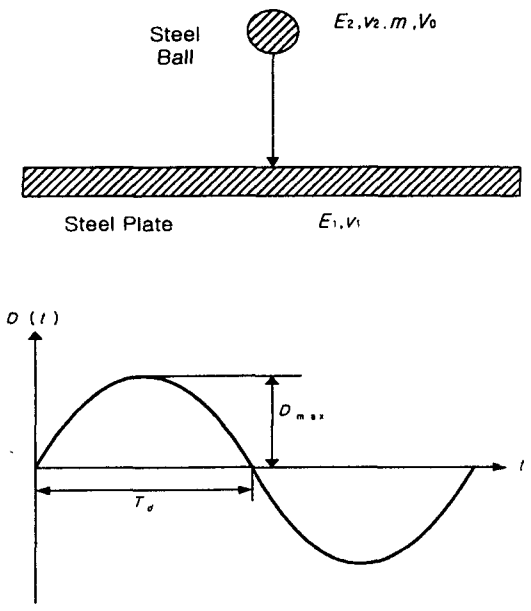

Fig. 2. Clash Test and the Impact Waveform

2. Hertz Impact Theory and the Assumption of Sinusoidal Waveform

2.1. Hertz Impact Theory

The Hertz theory describes the impact of a solid sphere on metal infinite plate. The theory is based on the assumption that the principal response of the plate is a bending wave of a half period equal to the duration of the impact. The experimental results support this theory when the diameters of the sphere are not large compared to the thickness of the plate and when the impact velocity is sufficiently small to avoid plastic deformation. Fig. 2 displays the sinusoidal waveform of the impact signal, when the clash test is performed.

Under the assumption of a sinusoidal waveform, the maximum amplitude (D_{max}) of the displacement and the contacting time (T_d) of the solid sphere are given by:

$$D_{max} = K_h (mV_0^2)^{0.4} R^{-0.2} \quad (1)$$

$$T_d \doteq 2.94 \frac{D_{max}}{V_0} \quad (2)$$

$$K_h = \left[\frac{15}{16} \left(\frac{1-\nu_1^2}{E_1} - \frac{1-\nu_2^2}{E_2} \right) \right]^{0.4} \quad (1.a)$$

where m is the mass of the sphere, R is the radius of the sphere , ν_1 and E_1 are Poisson' s ratio and Young' s Modulus for the plate, ν_2 and E_2 are Poisson' s ratio and Young' s Modulus for the sphere, and V_0 is the initial velocity of the sphere. In (2), it is noted that the Hertz theory defines the relationship between V_0 and T_d.

2.2. The Assumption of a Sinusoidal Waveform

Elastic or near-elastic impacts between metal objects and a metal plate are generally characterized by the contact force trajectory which is very close to the half-sine function [8]. Also, it is well known that the acceleration of the impacting object during contact is proportional to the applied force through Newton' s second law of motion. This relationship and the maximum displacement predicted by the Hertz theory, in turn, lead to the resultant equations of the object' s motion, where D(t), V(t) and A(t) denote the displacement, velocity and acceleration, respectively.

$$D(t) = D_{max} \sin\left(\frac{\pi}{T_d} t\right) \quad (3)$$

$$V(t) = D'(t) = \frac{\pi}{T_d} D_{max} \cos\left(\frac{\pi}{T_d} t\right) \quad (4)$$

$$A(t) = D''(t) = -\left(\frac{\pi}{T_d}\right)^2 D_{max} \sin\left(\frac{\pi}{T_d} t\right) \quad (5)$$

Then, using (5), the contact force is obtained as

$$F(t) = mA(t) \quad 0 < t < T_d \tag{6}$$

From (4), the maximum velocity would be

$$V_{max} = V(0) = V_0 = \pi / T_d \, D_{max} , \tag{7}$$

That is, the contact time Td is given by

$$T_d = \pi \, D_{max} / V_0 \tag{8}$$

Comparing (2) with (8), (2) differs from (8) by a factor of $\pi/2.94(\cong 1.6)$. Hence, in accordance with the half-sine interpretation, the Hertz theory based calculation needs to be adjusted by this factor.

3. Mass Estimation Algorithm

3.1. Regulation of a Half Period

Fig. 3 shows the flowchart of the developed algorithm. In this fig., the input parameters are the maximum amplitude of the impact signal (g), initial half period (sec), distance (m), impact velocity (m/sec) and thickness (m). From the flowchart, we know that the basic algorithm of the Hertz theory is modified by revising it experimentally. The basic algorithm is only one way at the modification part. That is, the basic algorithm only assumes that the plate is infinite and the impact signal is a sinusoidal waveform. So the basic algorithm only calculates eqn (8). Practically, the real plant structure is finite and the structure shape is cylindrical and hemispherical. Through many tests, three half period branches are set to adjust the weighting factor according to a scope of the initial half period. Fig. 4 shows the sequence of the initial half period and Table 1 summarizes the scope of the initial half-period and weighting factor.

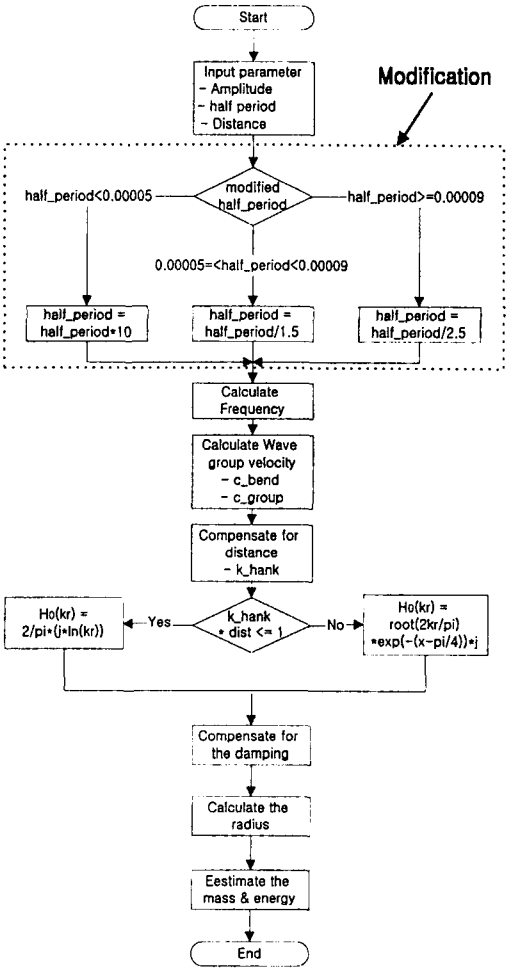

Fig. 3. The Developed Mass Estimation Algorithm

Table 1. Scope of the Initial Half-period and Weighting Factor

Scope	Weighting factor	Adjusting Value
Half-period < 0.0005	10	Half-period × 10
0.0005<Half-period<0.0009	0.67	Half-period × 0.67
Half-period >0.0009	0.4	Half-period × 0.4

3.2. Compensation for the Attenuation Effects

3.2.1. Wave Propagation Along the Plate

The solution for the two dimensional waves propagating from a localized force were given by Lamb[9] and after amplitude normalization, it can be used to calculate the plate surface acceleration wave shape as a function of impacting object mass and velocity. However, it is very difficult to do due to the nonlinear nature of the equation. A simpler alternative is to assume that the acceleration wave consists primarily of a few half periods at a frequency 1.6 times more than that of the observed actual signals. The magnitude of this signal is set to the plate acceleration waveform. The force and the acceleration at the sphere' s point are related by

$$A_{plate} = F_{max}/m = k_h^{-1} m^{-0.4} V_0^{1.3} R^{0.2} \quad (9)$$

Redefining into the plate' s point, (9) becomes

$$A_{plate} = F_{max}/M_{eff} \quad (10)$$

where F_{max} is the maximum impact force and M_{eff} is the effective mass of the plate.

Note that the same force term F_{max} is used in (9) and (10), while the mass term, m, in (9) is replaced by Meff in (10). The effective mass of the plate volume responding during the contact time is given by

$$M_{eff} = \pi (C_b T_d)^2 h \rho_{steel} \quad (11)$$

$$C_b = C_L (1.8hf_a / C_L + 4.5hf_a)^{0.5} \quad (12)$$

where C_b is the phase velocity of the bending wave in a steel plate, f_a is the frequency of interest

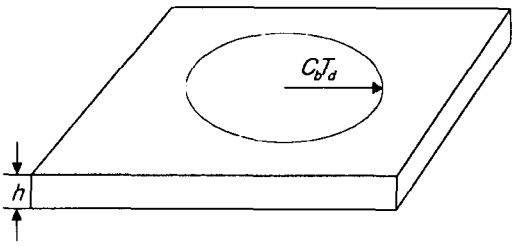

Fig. 4. The Effective Mass of the Plate

in Hz, C_L is 5,270 m/sec, T_d is the contact time, h is the plate thickness and ρ_{steel} is the density of the plate. Fig. 5 shows the effective mass of the plate.

3.2.2. Distance Attenuation and Damping Loss

In (10), we calculate the mass estimation for the case that the impact point is equal to the installed sensor position. In general, since the sensor position does not coincide with the impact point, it is necessary to compensate for damping and distance attenuation. A transverse impact against a plate excites a cylindrical wave whose radius increases with time as the wave propagates away from the impact point. The amplitude of this wave decreases as a function of the distance due to the increasing area covered by the wave and energy losses, referred to as damping.

The distance attenuation occurs when the impact signal is propagating from the impact point to the sensor location. The characteristic of the impact signal can be expressed as many values of kr (k is the wave number and r is the distance) with asymptotic approximations with the Hankel function. Eqn. (13) expresses the relationship between distance and amplitude. The decrease in amplitude of a plate' s bending wave is proportional to an increase in the distance from the impact source.

$$D(r) = D_0\left[H_0(kr) - H_0(-jkr)\right] \quad (13)$$

where D(r) is the wave amplitude at a distance r, D_0 is the amplitude at the point of impact, k is the wave number $2\pi f/D_o$, H_0 is the Hankel function of the 2nd kind, $H_o(kr) = 2j/\pi \ln(kr)$ $\{|kr| \ll 1\}$, $H_o(kr) = (2kr/\pi)^{0.5} \exp(-j(x - \pi/4))$ $\{|kr| \gg 1\}$.

Impact wave attenuation during propagation also occurs due to the internal energy dissipation along the plate and the radiation energy to the surrounding fluids. Eqn. (14) expresses this type of loss for bending waves.

$$D(r) = D_0 e^{-\left(\frac{\pi\eta f}{C_g}\right)r} \quad (14)$$

where D_0 is the initial amplitude, η is the loss factor defined in (15), f is the frequency of interest, γ is the distance traveled and C_g is the bending wave group velocity given by (16)

$$\eta = \frac{\rho_0 c_0}{2\pi f \rho_s h} \times \frac{M_f}{\sqrt{M_f^2 - 1}} \quad (15)$$

$$C_g = \frac{3.6 C_{fl} h_f}{C_b\left(C_{fl} + 9 h_f\right)} \quad (16)$$

4. Analysis Results

4.1. Test Environment

The impact test environment needs to be the same as that of normal operation. So, the reactor status must be more than hot standby. That is, RCP 1 was operating because the temperature was fixed to 100℃. The number of impact tests at each sensor was about six. The tool of the impact test was an impact ball, 530 grams. The internal flow velocity within the S/G was 1.0844m/sec and the sensor's sensitivity was 10pC/g through 50pC/g. The starting point of impact was applied to the A_0 mode wave

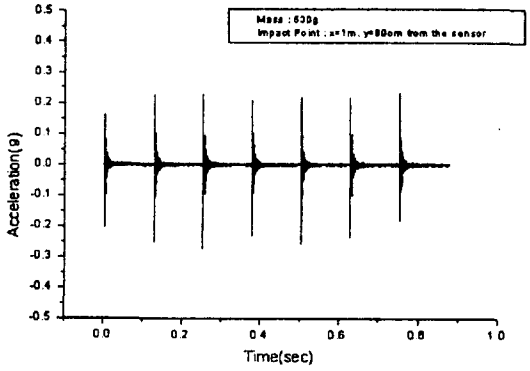

Fig. 6. Impact Signal

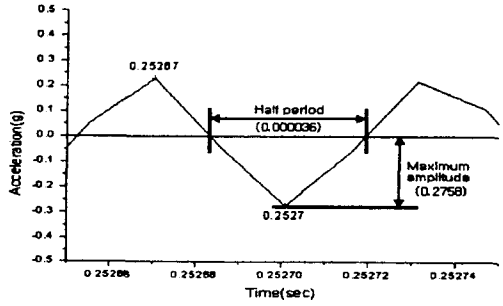

Fig. 7. Maximum Amplitude and Half Period

(Transverse wave). The recorder used was TEAC RD-135T. The sampling time of the recorder was 512KHz ($1/\Delta t = 1.9539 \times 10^{-5}$) and the S/N ratio was 72dB.

The impact data was collected from sensors 6, 7 and 8 at S/G 1 and sensors 10, 11 and 12 at S/G 2. Among these sensors, the impact test occurred at sensor 6, 8 and 12. Fig. 6 shows an impact signal of the impact data using the ORIGIN Tool. Fig. 7 describes the extension of Fig. 6 for analysis. In figs. 6 & 7, the initial half-period is 36 μsec and the maximum amplitude is 0.2758 g.

Fig. 8 shows the calculation part of the automatic mass estimation. In this figure, the left side puts in the input parameters and the right side

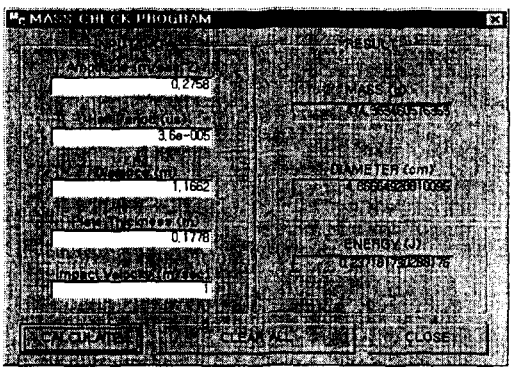

Fig. 7. Mass Estimation Program

Table 2. The Result Between Calculated Mass and Actual Mass, Error

T. No	Amplitude (g)	Half period (μsec)	Judge radius (cm)	Judge mass (gram)	Actual mass (gram)	Error (%)
1	0.2758	36	4.8667	474.37	530	10.5
2	0.2466	38	4.6323	409.09	530	22.8
3	0.2594	30	4.9610	502.50	530	5.2
4	0.3318	35	5.2129	583.00	530	10
5	0.4291	35	5.6928	759.26	530	43.3
6	0.1634	46	3.3605	156.18	530	70.5
A.E						27.05

T. No : Test Number, A.E: Average Error

shows this result. From the figure, we see the calculation result is 474.36 gram and the radius is judged to be 4.8667cm but the actual mass is 530 gram. Therefore, the error is 10.5 %. Table 2 shows the result between the calculated mass, actual mass and error. According to Table 2, the average error is about 27.05 %. Even if the estimated results are more or less different from the actual value, our results are thought to be good enough taking the actual environment in account (each sensor and the structure's nonlinear characteristic, and the environmental effects).

5. Conclusions

In the conventional LPMS, the operators must have much knowledge for analyzing the impact signal and mass estimation. In this work, we have developed an automatic mass estimation algorithm and applied it to the impact tests at YGN 3. The result was approximately below a 27 % error rate between the actual mass and the estimated mass.

From the applications point of view, the developed algorithm is expected to provide the operators with more accurate estimation results contributing to enhanced safety and the prevention of accidents in a NPP.

Further Research is needed with the algorithm for finding out the automatic mass estimation without the operator's judgement. Also, new technology (for example, a neural network and wavelet transformation) will apply to the LPMS.

Acknowledgement

This work has been carried out under the Nuclear R&D program supported by MOST.

References

1. ASME-OM-SG Part12, Loose Parts Monitoring in Light-Water-Reactor Power Plant, (1997).
2. Joseph A. Thie, Power Reactor Noise, American Nuclear Society (ANS),(1981).
3. Charles W. Mayo, "Loose part signal theory", Progress in Nuclear Energy, Vol. 15, pp. 535-543, (1983).
4. B. J. Olma," Source Location and mass Estimation in Loose Parts Monitoring of mass estimation algorithm LWRs." Progress in Nuclear Energy, Vol. 15,(1985).
5. T. Tsunoda, et al, " Studies on the Loose part Evaluation Technique", Progress in Nuclear Energy, Vol. 15, (1985).

6. B. J. Olma and B. Schutz, " Advanced Burst Processing Methods in Loose Parts Monitoring", SMORN V, Progress in Nuclear Energy, Vol. 21, pp. 525-535, (1987).
7. Mayo, " Loose Part Mass and Energy Estimation", Progress in Nuclear Energy, Vol.34, pp. 263-282, (1999).
8. Mayo C. W. et al, Loose Parts Monitoring System Improvements, EPRI NP-5743, Final Report,(1988).
9. H.Lamb, "On Wave-propagation in Two Dimensions", Proceedings of the London Mathematical Society, Vol. 35,1920,pp.141-161,(1924).